Neural Network Model for Estimation of the Induced Electric Field during Transcranial Magnetic Stimulation

Oluwaponmile F. Afuwape [1,2], Olumide O. Olafasakin [2], David C. Jiles [1], *Life Fellow, IEEE*

[1] *Department of Electrical and Computer Engineering, Iowa State University, Ames, IA 50011, USA*
[2] *Department of Mechanical Engineering, Iowa State University, Ames, IA 50011, USA*
Author correspondence: oafuwape@iastate.edu

Transcranial Magnetic Stimulation (TMS) is a non-invasive neuromodulation technique with applications in brain mapping and effective neuronal connectivity. In its repetitive mode, it is used for the treatment of neurological and psychiatric disorders. It functions on the principle of electromagnetic induction, where generated magnetic fields (H-field) induce electric field (E-field) that stimulates the brain's neurons. With TMS studies, accurate estimation of the induced E-field is usually necessary. However, this requires a lot of processes, including the three-dimensional head model generation from magnetic resonance images (MRI) using the SimNIBS software and finite element analysis to calculate the induced E-field. These processes are time-consuming and computationally expensive. Additionally, with each head model's uniqueness, outcomes cannot be generalized across a particular population as the intensity of E-field is subject-specific. In this research, the authors develop deep convolutional neural network (deep CNN) models to determine the intensity of the induced E-field directly from the patient's MRI scan and across different coil types. We trained CNN models from anatomically realistic head models and across 16 coil types to predict the induced E-field in the brain and scalp (E-Max brain and scalp), and the volume of stimulation of the brain and scalp (V-half brain and scalp) from T1-weighted MRI scans. Using a deep CNN model, the processing time for estimating the induced E-field is significantly reduced, which is helpful both to clinicians and researchers as the need to create subject-specific anatomical head structures is eliminated. Also, there will be no need for additional stimulation sessions with the different coil types for TMS patients as the deep CNN model can predict the outcome from each coil type. The other advantage of the deep CNN model is that the E-field from the different coil types can be compared simultaneously.

***Index Terms*— Deep Convolutional Neural Network (Deep CNN), Induced Electric Field, MRI Scans, Transcranial Magnetic Stimulation (TMS)**

I. Introduction

Transcranial Magnetic Stimulation (TMS) is a non-invasive method of stimulating the neurons of the brain. TMS is based on Faraday's law of electromagnetic induction: a time-varying magnetic field is generated when pulses of current flow through coils made from copper wires and plastic insulation casings. This transient magnetic field (H-field), in turn, induces an electric field (E-field) capable of activating the brain's neurons [1].

TMS has been approved by the United States Food and Drug Administration (FDA) for motor mapping and studying cortical functions before surgeries and also for the treatment of neuropsychiatric disorders such as major depressive disorders (MDD) and obsessive-compulsive disorders (OCD). In its repetitive mode, it is used for the treatment of spinal cord injury and stroke. It is also currently been considered for the treatment of Parkinson's disease and Alzheimer's [2]. TMS is also used as a research tool for brain mapping and studying the structural and functional connectivity of the brain's neurons [3]. There are other methods for treating neuropsychiatric disorders, like drug therapy and deep brain stimulation. However, these other treatment methods are invasive, risky, or have specific side effects [4].

The brain is very complex as the interaction between the various neurons in the brain is complicated. Understanding the complex interconnections between the brain's neurons and how TMS impacts the broader functional network of the brain, remains a research topic in neuroscience and TMS studies [5].

TMS treatment's effect and outcome vary with patients even when stimulation is at the same anatomical location [6], [7]. One explanation for this uniqueness is the differing neuroanatomy of the subjects, and the varying structural and functional connectivity of the brain tissues, contributing to the spatial variation of the induced E-field during TMS [8], [9]. The response from individual subjects during TMS is also related to the brain's oscillatory activity before and during treatment [4], contributing to the temporal variation of the induced E-field during TMS. Other variations may arise from the incorrect targeting of the anatomical location, especially when navigated TMS (nTMS) technique is not employed [10]. There are also no neurophysiological measures to define the exact stimulated location for each patient. Understanding the mechanism of TMS, especially the spatiotemporal distribution of the induced E-field, therefore, becomes crucial in TMS research and clinical application. Techniques such as electroencephalography (EEG) [11] and functional magnetic resonance imaging (fMRI) [12] have been employed in various studies with TMS to observe the propagation of the induced E-field in the brain. The need, however, still arises for the quantitative estimation of the induced E-field, especially for industries involved in the manufacture and commercialization of TMS coils.

The study of the effect of varying coil design on the resulting induced E-field is also crucial as ascertaining the safety of patients and the effectiveness of TMS in treating neuropsychiatric disorders is required [13]. With TMS coil design, there is usually a trade-off between penetration depth and focality. Achieving focality of the induced E-field is of utmost importance in TMS treatment as this guides against stimulation of non-target areas [14]. As conventional coil

designs have only been able to stimulate superficial regions of the brain, another factor for consideration in TMS coil design is the rate of attenuation of the induced E-Field [15]. The attenuation rate with conventional coils is relatively high; hence, activation of the neurons cannot be achieved at great depth. Achieving stimulation at great depth with conventional TMS coils requires an increase in stimulation intensity [12], which results in overstimulation of the tissues at the surface, leading to severe side effects [16]. Coil design for deep penetration will require that the induced E-field be delivered at a sufficient intensity [15].

Coil geometry, positioning, and orientation with respect to the brain tissues also influence TMS outcome [4]. Positioning of TMS coils at different stimulation sites results in varying modulating effects. Vink et al. confirmed that positioning of the TMS coil at the motor cortex could activate neuroanatomical regions correlated with motor activity as observed by the movement of the subject's thumb. Studying the effect of coil positioning during TMS is crucial as wrong/improper coil positioning could lead to unnecessary brain tissue stimulation [16].

Estimating the induced E-field during TMS requires a lot of processes (as shown in Fig. 1) which includes the three-dimensional (3D) head model generation from magnetic resonance imaging (MRI) scans. Spherical head models have also been used in TMS E-field estimation studies. One challenge with the spherical head model is that the columnar structure of the brain (gyri and sulci), the unique curvature of the head model, the different tissues within the brain and their associated electrical properties are not considered, which affects the accuracy of the E-field intensity [17]. Head model generation from MRI scans has been made possible using the SimNIBS software, which takes about 4 hours for a complete head model conversion [18]. After the conversion, finite element analysis (FEA) is conducted to estimate the induced E-Field. This requires a few hours for completion, especially as it depends on the voxel sizes (resolution) of the model's tissues [19], [20]. These processes are time-consuming and computationally expensive. Additionally, with each head model's uniqueness, outcomes cannot be generalized across a particular population as the intensity of E-field is subject-specific.

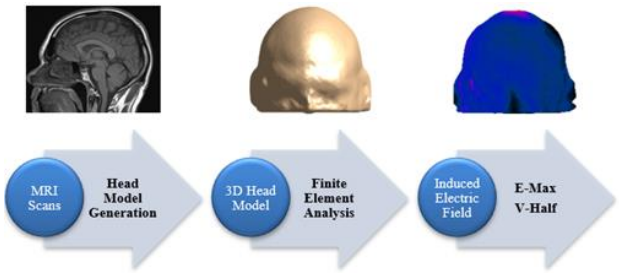

Fig. 1. Conventional process for the estimation of the induced electric field

Seeing these processes are time-consuming, we propose using a deep convolutional neural network (deep CNN) to directly determine the induced E-field from the patient's MRI scans. We consider the effect of varying coil configurations on the induced E-field and predict the induced E-field in the brain and scalp (E-Max brain and scalp) and the volume of stimulation of the brain and scalp (V-half brain and scalp) from T1-weighted MRI. Until now, few studies have explored the use of artificial neural networks to estimate the E-field from MRI [21], [22], [23]; however, none has considered the effect of different coil configurations in their estimation. With this deep CNN model, the induced E-field estimation time and computational cost are measurably reduced. Using this model to test the subject-specific response to TMS treatment will help neuroscientists and neurosurgeons predict TMS outcomes even before treatment. Additionally, TMS patients will not be exposed to unnecessary stimulation as the deep CNN model can predict the responses with the different coils before starting treatment.

II. Method

A. Human Models

T1-weighted MRI scans of 50 healthy adult subjects with ages ranging from 25-35 years were sourced from the Human Connectome Project Library [24] and converted to 3D head models [25]. The images consisted of seven different anatomical layers; skin (sn), skull (sk), cerebrospinal fluid (csf), grey matter (gm), white matter (wm), cerebellum (cb), and ventricles (vn). The different anatomical layers' electrical properties were obtained from the Information Technologies in Society (IT'IS) foundation database [26].

B. Finite Element Analysis

Sixteen (16) different coil types designed for TMS were considered in this study. Some of these coils are commercially available, while others are novel designs. The 16 different coil types are MCF-B65 Butterfly Coil [27], D-B80 Butterfly Coil [27], Cool-125 Circular Coil [27], MC-B70 Butterfly Coil [27], Double 25 mm Coil [28], Halo Coil [29], 110 mm Double Cone Coil [28], Double 70 mm Coil [28], Single 90 mm Coil [28], QBC [30], 3D-42 [31], 3D-43 [31], 3D-44 [31], Crown 39 [31], Crown 38 [31] and Crown 18 [31]. Finite element analysis (FEA) was conducted using an electromagnetic low-frequency solver, Sim4Life [32]. With this study, and depending on the configuration of each coil, the coils were positioned at the vertex or over the head of each of the 50 generated 3D head models. To simulate the TMS pulses, a current of amplitude 5000 A flowed through the coils at a frequency of 2.5 kHz. The direction of flow of the current was dependent on the configuration of each of the coils. The output from this simulation analysis is comparable to that of a conventional stimulator used for TMS treatment. With each coil, the analysis totaled up to 800 different simulations.

C. Data Interpretation

Results from Sim4Life were exported to MATLAB for postprocessing and interpretation of data. Four parameters, the maximum E-field intensity on the scalp (E-Max scalp), maximum E-field intensity on the brain (E-Max brain), the volume of the scalp stimulated (V-half scalp), and the volume of the brain stimulated (V-half brain), were calculated for each

of the 50 head models. The V-half is the volume of the scalp and brain exposed to at least half of the intensity of the maximum induced E-field.

D. Deep Convolutional Neural Network Model

Deep learning techniques to estimate the response variable y (E-max scalp, E-max brain, V-half scalp, and V-half brain) using the T1-weighted MRI (X) and the specific coil type (C) as explanatory variables were employed in this study. The model aims to solve the non-linear regression problem y = f (X, C, β). Deep CNN has been reported to help predict complex and non-linear regression problems [22]. The deep CNN models pipeline includes data preprocessing, model training, model evaluation, and model deployment. The model was developed using the TensorFlow Kera's toolkit [33].

i. Data Preprocessing

The images used for the Sim4life simulations are 3D MRI of size 260 X 311 X 260. The center slice of the 3D MRI was extracted and reshaped to 128 X 128 pixels to reduce the computational complexity of the CNN models. The images were rotated about the center at 90° intervals (90, 180, and 270°), increasing the input-output pairs (N) to 3200. The MRI were standardized by dividing all pixels by the maximum pixel in the dataset (0 ≤ pixels ≤ 1). The coil types were encoded using the one-hot encoding function from sci-kit learn, which converted the categorical variables into binary forms, fed into the deep CNN model. The 3200 input-output pairs were shuffled and split into learning pairs and test set at a ratio of 8:2. The learning pairs were further divided into training and validation sets at a ratio of 9:1, which resulted in 2304 pairs for the training set, 256 pairs for the validation set, and 640 input-output pairs for the test set. The training set and validation set were used to train the models, while the test set was used to evaluate the model.

ii. Model development and training

The deep CNN models consisted of five two-dimensional (2D) convolution layers (Fig. 2) with padding, which ensured the convolutional layer captured all information in the image and maintained the image dimensions at the layer's output. Three max-pooling layers with a pool size of 2 were introduced to reduce the spatial dimensions of the images. These layers pooled the pixels and kept the most important features of the images. Two fully connected hidden dense layers with drop-out layers were used to reduce overfitting. Finally, a neuron was built in the output layer. Rectified linear units (RELU) were used in all convolutional and fully connected hidden layers, while linear transfer function was used in the output layer to estimate the response variable. The models were trained and validated using the training set and validation set. The adaptive moment (Adams) estimation optimization technique was employed to optimize the model parameters. In developing the model, the input images of size 128 X 128 were fed into the first 2D convolution layer connected to other layers, as shown in Fig. 2. The coil type, C, was introduced into the algorithm after the MRI, X, had gone through all the convolutional layers and the output flattened. The coil type C was concatenated with the flattened output from the last max-pooling layer to get an array fed into the first fully connected dense layer. The model was compiled with mean square error (MSE) as the metrics, and an early stopping option was included to ensure that the algorithm stopped training when the model does not get better after 100 iterations.

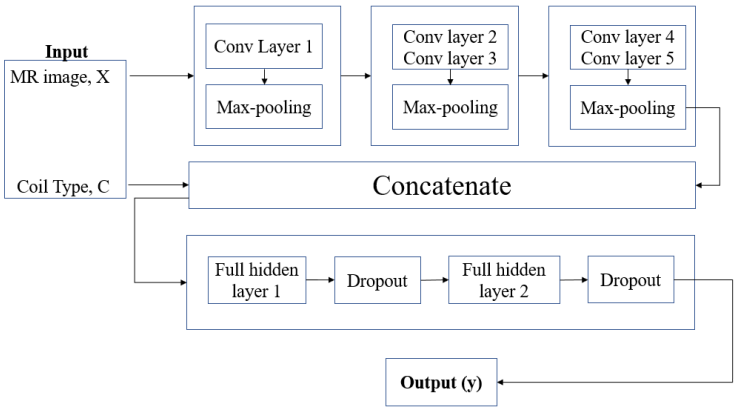

Fig. 2. Model architecture

$$z = (\mathrm{X} * \beta + \mathrm{b})$$

$$ReLU, R(z) = \begin{cases} z, & z \geq 0 \\ 0, & z < 0 \end{cases}$$

$$Linear\ , f(z) = z$$

Where:

X = the input data,
β = the model weights and
b = the bias.

iii. Model Evaluation

The performance of the deep CNN models was evaluated by comparing the predicted values, $\bar{y}_i$ with the simulated values from FEA using the coefficient of determination (R-square, R^2) and the mean absolute percentage error (MAPE). The R^2 value indicates the proportion of the variance in the dataset explained by the model. A score closer to 1 indicates a very good generalization, while a low R^2 value shows that the model does not explain the variation in the model.

$$\mathrm{R}^2 = 1 - \frac{\sum_{i=1}^{n}(\bar{y}_i - y_i)^2}{\sum_{i=1}^{n}(\bar{y}_i - \bar{y})^2}$$

The MAPE estimates the percentage difference between the predicted value and the simulated value. The MAPE represents the most relative meaningful estimation of the model's error.

$$\mathrm{MAPE} = \frac{1}{n}\sum_{i=1}^{n}\frac{|y_i - \bar{y}_i|}{y_i} * 100\ \%$$

Where:

$\bar{y}_i$ = the predicted value
y_i = the simulated value from FEA
$\bar{y}$ = the mean of the simulated values

III. Results and Discussion

The deep CNN models were trained to predict the E-Max scalp, E-Max brain, V-half scalp, and V-half brain. The MAPE and the R^2 were assessed based on the accuracy of the deep CNN model's predictions when compared to the FEA values (Sim4life's values). TABLE 1 summarizes the R^2 and MAPE values for the training and test data set of the four parameters.

a. E-Max scalp

The model recorded an R^2 value of 0.96 and 0.92 on the training and test set, respectively. The R^2 showed that the model explained about 96 % and 92 % of the actual and predicted values variation in the training and test set, respectively. This confirms that the model generalized well on the dataset and did not overfit the training set. The R^2 value recorded is comparable to the average R^2 value recorded in Yokota et al. [22]. The model also recorded a MAPE of 4.7 % and 6.2 % on the training and test set, respectively. The MAPE values further emphasized that the model generalized well on the dataset and did not overfit the training set. The parity plot for the training and test data set is presented in Fig. 3.

b. E-Max brain

The model recorded an R^2 value of 0.98 and 0.96 on the training and test set, respectively. The R^2 showed that the model explained about 98 % and 96 % of the actual and predicted values variation in the training and test set, respectively. The model also recorded a MAPE of 7.4 % and 9.3 % on the training and test set. The R^2 score and the MAPE values indicated an excellent generalization on the dataset and showed the model did not overfit the training set. The parity plot for the training and test data set is presented in Fig. 3.

TABLE 1. Summary of R^2 and MAPE values for the training and test dataset.

	Training		Test	
	R-square	MAPE	R-square	MAPE
E-max scalp	0.96	4.70 %	0.92	6.20 %
E-max brain	0.98	7.40 %	0.96	9.30 %
V-half scalp	0.63	220 %	0.47	250 %
V-half brain	0.72	133 %	0.59	138 %

c. V-half scalp

The model recorded an R^2 score of 0.63 and 0.47 on the training and test set, respectively. The model recorded a MAPE of 220 % and 250 % on the training and test set, respectively. The model performed poorly on the dataset and failed to generalize well while predicting the training and test set. One of the reasons for this poor performance could be the small size of the data sets, especially since the magnitude of the V-half parameters is really low. The parity plot for the training and test data set is presented in Fig. 3.

d. V-half brain

The model recorded an R^2 score of 0.72 and 0.59 on the training and test set, respectively. The R^2 shows that the model could not explain a significant part of the variation in actual and predicted values. The model also recorded a MAPE of 133 % and 138 % on the training and test set. Like the V-half scalp, the very poor MAPE is not surprising, giving the R^2 value was also not impressive. Although the model did not overfit the training set, it poorly predicted the training set and the test set. The parity plot for the training and test data set is presented in Fig. 3.

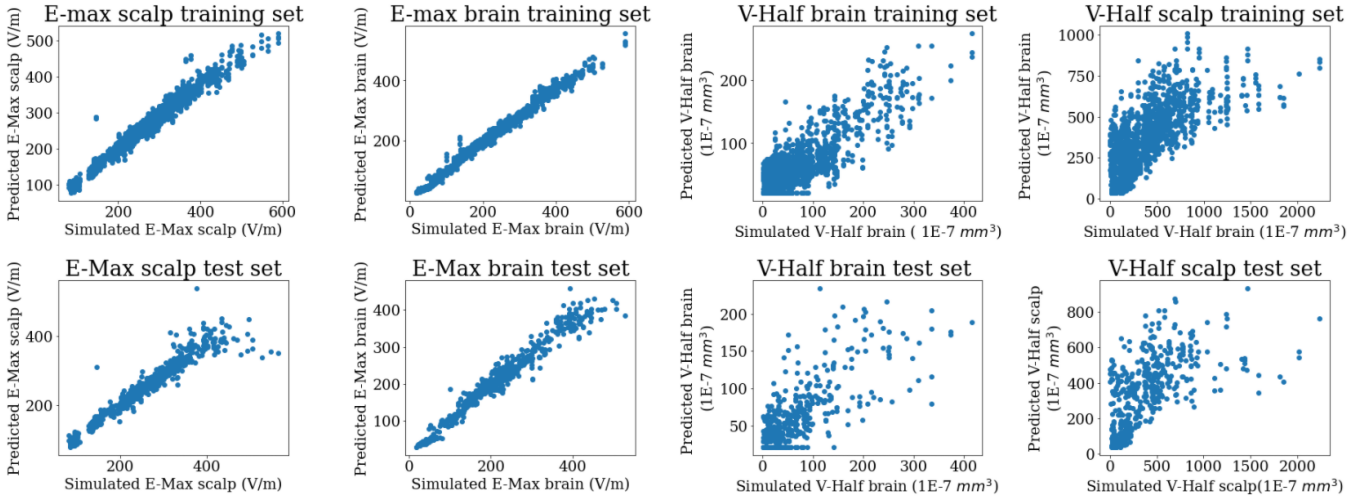

Fig. 3. Parity plot for the four parameters (training and test data set)

IV. Conclusion

This study is the first to report the use of deep CNN in accounting for the effect of different coil configurations on TMS outcomes. With the induced E-field values calculated for 50 head models and across 16 coil types, the deep CNN model was successfully trained to predict the four parameters of the induced E-field (E-Max brain, E-Max scalp, V-half brain, and V-half scalp). The R^2 and MAPE values have been reported for all the parameters. We plan to develop deep CNN models using the full-pixel sizes of the 3D MRI to take advantage of all the information in the images in the future (we have only used the center slice of the MRI in this present study). We also plan to use a larger dataset to develop a good model for the V-half parameters.

ACKNOWLEDGMENT

This research is funded by the Barbara and James Palmer Foundation and the Stanley Chair in Interdisciplinary Engineering at Iowa State University.

REFERENCES

[1] O. F. Afuwape, H. Oya, A. D. Boes, and D. C. Jiles, "Measurement and Modeling of the Effects of Transcranial Magnetic Stimulation on the Brain," *IEEE Transactions on Magnetics*, pp. 1–1, 2020, doi: 10.1109/TMAG.2020.3008554.

[2] L. J. Gomez, S. M. Goetz, and A. V. Peterchev, "Design of transcranial magnetic stimulation coils with optimal trade-off between depth, focality, and energy," *J. Neural Eng.*, vol. 15, no. 4, p. 046033, Aug. 2018, doi: 10.1088/1741-2552/aac967.

[3] M. Hallett, "Transcranial magnetic stimulation and the human brain," *Nature*, vol. 406, no. 6792, pp. 147–150, Jul. 2000, doi: 10.1038/35018000.

[4] J. J. T. Vink, S. Mandija, P. I. Petrov, C. A. T. van den Berg, I. E. C. Sommer, and S. F. W. Neggers, "A novel concurrent TMS-fMRI method to reveal propagation patterns of prefrontal magnetic brain stimulation," *Hum Brain Mapp*, vol. 39, no. 11, pp. 4580–4592, Aug. 2018, doi: 10.1002/hbm.24307.

[5] E. Tang and D. S. Bassett, "*Colloquium* : Control of dynamics in brain networks," *Rev. Mod. Phys.*, vol. 90, no. 3, p. 031003, Aug. 2018, doi: 10.1103/RevModPhys.90.031003.

[6] O. Afuwape, P. Rastogi, and D. Jiles, "Comparison of the Effect of Coil Configuration and the Variability of Anatomical Structure on Transcranial Magnetic Stimulation," *IEEE Transactions on Magnetics*, pp. 1–1, 2020, doi: 10.1109/TMAG.2020.3006459.

[7] L. J. Crowther, R. L. Hadimani, and D. C. Jiles, "Effect of Anatomical Brain Development on Induced Electric Fields During Transcranial Magnetic Stimulation," *IEEE Transactions on Magnetics*, vol. 50, no. 11, pp. 1–4, Nov. 2014, doi: 10.1109/TMAG.2014.2326819.

[8] F. Syeda, H. Magsood, E. G. Lee, A. A. El-Gendy, D. C. Jiles, and R. L. Hadimani, "Effect of anatomical variability in brain on transcranial magnetic stimulation treatment," *AIP Advances*, vol. 7, no. 5, p. 056711, Jan. 2017, doi: 10.1063/1.4974981.

[9] P. C. Miranda, L. Correia, R. Salvador, and P. J. Basser, "The Role of Tissue Heterogeneity in Neural Stimulation by Applied Electric Fields," in *2007 29th Annual International Conference of the IEEE Engineering in Medicine and Biology Society*, Aug. 2007, pp. 1715–1718. doi: 10.1109/IEMBS.2007.4352640.

[10] H. Hannula and R. J. Ilmoniemi, "Basic Principles of Navigated TMS," in *Navigated Transcranial Magnetic Stimulation in Neurosurgery*, S. M. Krieg, Ed. Cham: Springer International Publishing, 2017, pp. 3–29. doi: 10.1007/978-3-319-54918-7_1.

[11] C. Zrenner, D. Desideri, P. Belardinelli, and U. Ziemann, "Real-time EEG-defined excitability states determine efficacy of TMS-induced plasticity in human motor cortex," *Brain Stimulation*, vol. 11, no. 2, pp. 374–389, Mar. 2018, doi: 10.1016/j.brs.2017.11.016.

[12] C. C. Ruff, J. Driver, and S. Bestmann, "Combining TMS and fMRI," *Cortex*, vol. 45, no. 9, pp. 1043–1049, Oct. 2009, doi: 10.1016/j.cortex.2008.10.012.

[13] S. Zibman, G. S. Pell, N. Barnea-Ygael, Y. Roth, and A. Zangen, "Application of transcranial magnetic stimulation for major depression: Coil design and neuroanatomical variability considerations," *European Neuropsychopharmacology*, Jul. 2019, doi: 10.1016/j.euroneuro.2019.06.009.

[14] Shuo Yang *et al.*, "3D realistic head model simulation based on transcranial magnetic stimulation," in *2006 International Conference of the IEEE Engineering in Medicine and Biology Society*, Aug. 2006, vol. Supplement, pp. 6469–6472. doi: 10.1109/IEMBS.2006.260877.

[15] Y. Roth, A. Zangen, and M. Hallett, "A Coil Design for Transcranial Magnetic Stimulation of Deep Brain Regions:," *Journal of Clinical Neurophysiology*, vol. 19, no. 4, pp. 361–370, Aug. 2002, doi: 10.1097/00004691-200208000-00008.

[16] L. Hernandez-Garcia, T. Hall, L. Gomez, and E. Michielssen, "A numerically optimized active shield for improved transcranial magnetic stimulation targeting," *Brain Stimulation*, vol. 3, no. 4, pp. 218–225, Oct. 2010, doi: 10.1016/j.brs.2010.05.001.

[17] A. M. Samoudi, E. Tanghe, L. Martens, and W. Joseph, "Deep Transcranial Magnetic Stimulation: Improved Coil Design and Assessment of the Induced Fields Using MIDA Model," *BioMed Research International*, Jun. 05, 2018. https://www.hindawi.com/journals/bmri/2018/7061420/ (accessed Dec. 08, 2020).

[18] M. Windhoff, A. Opitz, and A. Thielscher, "Electric field calculations in brain stimulation based on finite elements: An optimized processing pipeline for the generation and usage of accurate individual head models," *Human Brain Mapping*, vol. 34, no. 4, pp. 923–935, 2013, doi: 10.1002/hbm.21479.

[19] A. Opitz, W. Legon, A. Rowlands, W. K. Bickel, W. Paulus, and W. J. Tyler, "Physiological observations validate finite element models for estimating subject-specific electric field distributions induced by transcranial magnetic stimulation of the human motor cortex," *Neuroimage*, vol. 81, pp. 253–264, Nov. 2013, doi: 10.1016/j.neuroimage.2013.04.067.

[20] N. J. Tachas, K. G. Efthimiadis, and T. Samaras, "The Effect of Coil Modeling on the Predicted Induced Electric Field Distribution During TMS," *IEEE Transactions on Magnetics*, vol. 49, no. 3, pp. 1096–1100, Mar. 2013, doi: 10.1109/TMAG.2012.2219878.

[21] J. A. Livezey, K. E. Bouchard, and E. F. Chang, "Deep learning as a tool for neural data analysis: Speech classification and cross-frequency coupling in human sensorimotor cortex," *PLoS Comput Biol*, vol. 15, no. 9, p. e1007091, Sep. 2019, doi: 10.1371/journal.pcbi.1007091.

[22] T. Yokota *et al.*, "Real-time estimation of electric fields induced by transcranial magnetic stimulation with deep neural networks," *Brain Stimul*, vol. 12, no. 6, pp. 1500–1507, Dec. 2019, doi: 10.1016/j.brs.2019.06.015.

[23] A. S. Lundervold and A. Lundervold, "An overview of deep learning in medical imaging focusing on MRI," *Zeitschrift für Medizinische Physik*, vol. 29, no. 2, pp. 102–127, May 2019, doi: 10.1016/j.zemedi.2018.11.002.

[24] D. C. V. Essen *et al.*, "The Human Connectome Project: A data acquisition perspective," *NeuroImage*, vol. 62, no. 4, pp. 2222–2231, 2012, doi: https://doi.org/10.1016/j.neuroimage.2012.02.018.

[25] E. G. Lee *et al.*, "Investigational Effect of Brain-Scalp Distance on the Efficacy of Transcranial Magnetic Stimulation Treatment in Depression," *IEEE Transactions on Magnetics*, vol. 52, no. 7, pp. 1–4, Jul. 2016, doi: 10.1109/TMAG.2015.2514158.

[26] M.-C. Gosselin *et al.*, "Development of a new generation of high-resolution anatomical models for medical device evaluation: the Virtual Population 3.0," *Phys Med Biol*, vol. 59, no. 18, pp. 5287–5303, Sep. 2014, doi: 10.1088/0031-9155/59/18/5287.

[27] "Hs6bbeD6SsaHvLeg3403_501-0626 Magnetic Stimulation Accessories Catalogue UK-edition rev 6.5.pdf." Accessed: May 08, 2020. [Online]. Available: https://irp-cdn.multiscreensite.com/91b5b819/files/uploaded/Hs6bbeD6SsaHvLeg3403_501-0626%20Magnetic%20Stimulation%20Accessories%20Catalogue%20UK-edition%20rev%206.5.pdf

[28] "Magstim Coils Archives," *Magstim TMS*. https://www.magstim.com/product-category/coils/ (accessed Mar. 15, 2021).

[29] L. J. Crowther, P. Marketos, P. I. Williams, Y. Melikhov, D. C. Jiles, and J. H. Starzewski, "Transcranial magnetic stimulation: Improved coil design for deep brain investigation," *Journal of Applied Physics*, vol. 109, no. 7, p. 07B314, Apr. 2011, doi: 10.1063/1.3563076.

[30] P. Rastogi, E. G. Lee, R. L. Hadimani, and D. C. Jiles, "Transcranial Magnetic Stimulation-coil design with improved focality," *AIP Advances*, vol. 7, no. 5, p. 056705, May 2017, doi: 10.1063/1.4973604.

[31] Z.-D. Deng, S. H. Lisanby, and A. V. Peterchev, "Electric field depth–focality trade-off in transcranial magnetic stimulation: Simulation comparison of 50 coil designs," *Brain Stimulation*, vol. 6, no. 1, pp. 1–13, Jan. 2013, doi: 10.1016/j.brs.2012.02.005.

[32] E. Neufeld, M. C. Gosselin, D. Sczcerba, M. Zefferer, and N. Kuster, *Sim4Life: A Medical Image Data Based Multiphysics Simulation Platform for Computational Life Sciences*. 2012.

[33] M. Abadi *et al.*, "TensorFlow: A System for Large-Scale Machine Learning," in *12th USENIX Symposium on Operating Systems Design and Implementation (OSDI 16)*, Savannah, GA, Nov. 2016, pp. 265–283. [Online]. Available: https://www.usenix.org/conference/osdi16/technical-sessions/presentation/abadi